

On the Connection Between Differential Population Growth Rate and Epidemic Reproduction Numbers

Hong Qin*

School of Data Science, Department of Computer Science,
Old Dominion University, Norfolk, VA 23529, USA

ORCID: 0000-0001-9007-4622

Abstract

During pandemics, public health agencies need to rapidly assess whether a new viral variant is more transmissible than existing ones. When two viral variants co-circulate, their relative fitness can be quantified in several related ways: as a selective coefficient in the tradition of Kimura’s population genetics, as the differential population growth rate (DPGR) estimated from genomic surveillance data, or as a contrast in epidemic reproduction numbers R_t . We show that DPGR estimates a pairwise growth-rate difference. Under a specified generation-interval model, this growth-rate difference can be transformed into a contrast in reproduction-number space; in the equal-generation-time SIR special case, the relationship reduces to a scaled difference in variant-specific R_t . Closely related growth-rate contrasts also appear inside multinomial logistic (softmax) and growth-advantage random walk (GARW) frameworks, although those methods differ from DPGR in likelihood structure, smoothing, priors, and data inputs. We evaluate the theory empirically across five analyses spanning SARS-CoV-2 (three analyses, $r = 0.56$ to 0.78) and influenza H1N1 and H3N2 (two analyses, $r = 0.31$ to 0.38), totaling over 2,200 matched data points, with SIR simulation confirming recovery of the expected mapping (slope = 0.99) when the true R_t is known. Applied retrospectively to five major SARS-CoV-2 variant transitions, sustained DPGR signals detected emerging fitness advantages 43 to 65 days before variant dominance, with 95% sign accuracy in our analysis. DPGR is approximately transitive across 115,624 variant triplets, consistent with an additive lineage-level growth-rate representation, approximately zero for selected functionally similar sub-lineages, and directionally consistent across 11 countries. The core algebraic statements are formalized in Lean 4 with Mathlib. These results connect sequence-count-based variant fitness estimates to reproduction-number contrasts through an assumption-explicit growth-rate bridge.

Keywords: variant fitness, reproduction number, differential population growth rate, population genetics, SARS-CoV-2, influenza, formal verification

1 Introduction

When a new viral variant is detected during a pandemic, public health agencies face an urgent question: will this variant outcompete existing ones, and if so, how quickly? Answering this currently requires fitting complex transmission models to absolute incidence data, estimating generation-time distributions, and waiting for sufficient case counts to accumulate. Yet the most rapidly available

signal is often the simplest: the relative abundance of variant sequences in routine genomic surveillance. If the mathematical relationship between sequence-derived fitness measures and epidemic reproduction numbers were made explicit, variant risk assessment could begin as soon as sequence data appear, weeks before traditional epidemiological estimates become reliable.

The question of how to measure the relative fitness of competing biological types has a long history. In classical population genetics, Kimura showed that under deterministic selection in a large population, the log-ratio of two allele frequencies changes linearly in time at a rate equal to their selective coefficient difference (Kimura 1962). His neutral theory further established that $s = 0$ (no systematic trend in the log-ratio) is the null hypothesis against which selection is tested (Kimura 1968).

Six decades later, Pantho et al. (2025) independently arrived at the same mathematical structure in the context of viral genomic surveillance. Their differential population growth rate (DPGR) estimates the slope of $\log_{10}(N_i/N_j)$ over a sliding time window, which is the selective coefficient of classical theory, applied to co-circulating viral lineages (Pantho et al. 2025).¹ The DPGR framework has since been extended to influenza strain dominance across regions and seasons (Uddin et al. 2025), to predicting variant fitness from full viral genome sequences (Annan et al. 2025), and to genome-wide association analysis of fitness-linked mutations (Hatami et al. 2026).

Meanwhile, several groups have developed methods to estimate variant-specific fitness from sequence frequencies: Kimura et al.’s Bayesian multinomial logistic (softmax) model (Kimura et al. 2022), Figgins and Bedford’s growth-advantage random walk (GARW) (Figgins and Bedford 2025), and Obermeyer et al.’s PyR0 framework (Obermeyer et al. 2022). Each estimates a variant-specific growth advantage and converts it to a relative effective reproduction number R_e by assuming a generation-time distribution.

A natural question arises: how are these quantities (the classical selective coefficient, DPGR, and contrasts in epidemic reproduction numbers) related? We show that DPGR estimates the pairwise growth-rate contrast. Under a short-window two-variant SIR approximation, and conditional on shared susceptibility assumptions, DPGR maps to a scaled difference in variant-specific R_t (Proposition 1). Under a fixed-generation-time model, it maps to a scaled log-ratio of R_e values. More generally, for any monotone growth-rate-to-reproduction-number map Φ , DPGR induces a pairwise contrast only after the baseline growth rate and the map Φ have been specified (Proposition 2). Related growth-rate contrasts also appear inside softmax and GARW parameterizations. The core algebraic results are formalized in Lean 4 with Mathlib (Appendix), and evaluated empirically across five analyses spanning SARS-CoV-2 and influenza.

Throughout, R_t denotes the time-varying effective reproduction number in an SIR model, and R_e denotes the growth-rate-derived reproduction number via the Wallinga-Lipsitch mapping (Wallinga and Lipsitch 2007).

2 Population Genetics Foundation

The connection between DPGR and classical fitness theory is immediate. Consider two types i and j with fitnesses $w_i = 1 + s_i$ and $w_j = 1 + s_j$ in a large population under deterministic selection. After t generations, the frequency ratio evolves as

$$\frac{p_i(t)}{p_j(t)} = \left(\frac{w_i}{w_j}\right)^t \frac{p_i(0)}{p_j(0)},$$

¹In their application, time is measured in days and the regression is performed on a sliding time window chosen so that the log-ratio is approximately linear.

so

$$\ln\left(\frac{p_i(t)}{p_j(t)}\right) = t \ln\left(\frac{w_i}{w_j}\right) + C \approx (s_i - s_j)t + C, \quad (1)$$

where the approximation holds for small s . This is the classical result: the log-frequency ratio changes linearly with slope equal to the selective coefficient difference (Kimura 1962).

Comparing (1) with Pantho et al.'s definition (Pantho et al. 2025),

$$\log_{10}\left(\frac{N_i(t)}{N_j(t)}\right) = \text{DPGR}_{i,j} t + C,$$

we obtain

$$s_i - s_j = \ln(10) \text{DPGR}_{i,j}. \quad (2)$$

Thus DPGR is the classical selective coefficient, rescaled from natural to base-10 logarithms.

One important difference separates the two settings. Kimura's model assumes *constant* fitness: the selective coefficient s does not change over time. In an epidemic, however, susceptible depletion causes the effective fitness of each variant to change as immunity builds. The short-window approximation used by Pantho et al. recovers the Kimura regime: within each window, $S(t)/N$ changes slowly enough that the fitness difference is approximately constant, and the log-ratio is approximately linear. The time-varying R_t tracks how this fitness evolves across windows.

From Kimura's neutral theory (Kimura 1968), the null hypothesis is $s_i = s_j$, i.e., $\text{DPGR}_{i,j} = 0$. A statistically significant non-zero DPGR is therefore evidence of differential selection between the two lineages.

3 DPGR as a Difference in Growth Rates

Pantho et al. define DPGR through the pairwise log-ratio model

$$\log_{10}\left(\frac{N_i(t)}{N_j(t)}\right) = \text{DPGR}_{i,j} t + C, \quad (3)$$

where $N_i(t)$ and $N_j(t)$ are the two variant sub-populations in the chosen time window and C is a constant that absorbs lag effects and initial conditions.

Equation (3) is written in base-10 logarithms because that is the convention used in the DPGR paper. For epidemic modeling, it is often more convenient to work with natural logarithms and Malthusian growth rates. Writing

$$N_k(t) \approx A_k e^{r_k t}, \quad k \in \{i, j\}, \quad (4)$$

gives

$$\ln\left(\frac{N_i(t)}{N_j(t)}\right) = (r_i - r_j)t + C', \quad (5)$$

so that

$$r_i - r_j = \ln(10) \text{DPGR}_{i,j}. \quad (6)$$

Thus, up to the factor $\ln(10)$, DPGR is a *difference of growth rates*. If one instead fits the log-ratio using natural logarithms, the conversion factor disappears.

4 Two-Variant SIR Derivation

Consider a two-variant SIR-type model in a population of size N :

$$\frac{dS}{dt} = -\frac{S}{N}(\beta_i I_i + \beta_j I_j), \quad (7)$$

$$\frac{dI_i}{dt} = \left(\beta_i \frac{S}{N} - \gamma_i \right) I_i, \quad (8)$$

$$\frac{dI_j}{dt} = \left(\beta_j \frac{S}{N} - \gamma_j \right) I_j. \quad (9)$$

Here β_k is the transmission rate and γ_k is the removal or recovery rate for variant k .

Over a sufficiently short window, if $S(t)$ changes slowly compared with the window length, each infected sub-population is approximately exponential:

$$I_k(t) \approx I_k(t_0) \exp(r_k(t_0)(t - t_0)), \quad (10)$$

with local growth rate

$$r_k(t) = \beta_k \frac{S(t)}{N} - \gamma_k. \quad (11)$$

Define the variant-specific effective reproduction number by

$$R_{t,k} = \frac{\beta_k S(t)}{\gamma_k N}. \quad (12)$$

This definition has a direct epidemiological meaning:

- The factor $\beta_k S(t)/N$ is the instantaneous rate at which one infectious individual of variant k generates new infections at time t , after accounting for the fact that only the fraction $S(t)/N$ of the population remains susceptible.
- In the SIR model, $1/\gamma_k$ is the mean infectious period for variant k .
- Multiplying these two quantities gives the expected number of secondary infections caused by one infectious individual of variant k at time t , which is $R_{t,k}$.

Equivalently,

$$\beta_k \frac{S(t)}{N} = \gamma_k R_{t,k}.$$

Substituting this identity into (11), we obtain the growth-rate relation step by step:

$$\begin{aligned} r_k(t) &= \beta_k \frac{S(t)}{N} - \gamma_k \\ &= \gamma_k R_{t,k} - \gamma_k \\ &= \gamma_k (R_{t,k} - 1). \end{aligned} \quad (13)$$

Thus $R_{t,k} > 1$ corresponds to local exponential growth, $R_{t,k} < 1$ corresponds to decline, and $R_{t,k} = 1$ marks the threshold between the two.

Proposition 1 (SIR bridge from DPGR to R_t and R_0). *Under the two-variant SIR approximation,*

$$\text{DPGR}_{i,j}(t) = \frac{1}{\ln(10)} [\gamma_i(R_{t,i}(t) - 1) - \gamma_j(R_{t,j}(t) - 1)].$$

If moreover $S(t) = N$, so that $R_{0,k} = \beta_k/\gamma_k$, then

$$\text{DPGR}_{i,j}(t) = \frac{1}{\ln(10)} [\gamma_i(R_{0,i} - 1) - \gamma_j(R_{0,j} - 1)].$$

Substituting (13) into (6) yields the main connection recorded in Proposition 1:

$$\text{DPGR}_{i,j}(t) = \frac{1}{\ln(10)} [\gamma_i(R_{t,i} - 1) - \gamma_j(R_{t,j} - 1)]. \quad (14)$$

Equation (14) shows that DPGR is not itself a reproduction number. Rather, it is the *difference in transmission growth advantages* after translating reproduction numbers into exponential growth-rate space.

5 Important Special Cases

Common infectious period or generation time

If the two variants have approximately the same removal rate,

$$\gamma_i \approx \gamma_j \approx \gamma,$$

then (14) simplifies to

$$\text{DPGR}_{i,j}(t) \approx \frac{\gamma}{\ln(10)} (R_{t,i} - R_{t,j}). \quad (15)$$

With mean infectious period or generation time $T_g \approx 1/\gamma$, this can also be written as

$$\text{DPGR}_{i,j}(t) \approx \frac{R_{t,i} - R_{t,j}}{T_g \ln(10)}. \quad (16)$$

Therefore, under equal generation-time assumptions, DPGR is proportional to the *difference* in the variants' effective reproduction numbers.

Early epidemic or nearly fully susceptible phase

If susceptible depletion is negligible so that $S(t) \approx N$, then

$$R_{t,k} \approx R_{0,k} = \frac{\beta_k}{\gamma_k},$$

and (14) reduces to

$$\text{DPGR}_{i,j} \approx \frac{1}{\ln(10)} [\gamma_i(R_{0,i} - 1) - \gamma_j(R_{0,j} - 1)]. \quad (17)$$

If, in addition, $\gamma_i \approx \gamma_j \approx \gamma$, then

$$\text{DPGR}_{i,j} \approx \frac{\gamma}{\ln(10)} (R_{0,i} - R_{0,j}). \quad (18)$$

So in the early susceptible phase, DPGR is proportional to the difference in basic reproduction numbers.

6 Principled Interpretation

The main conceptual distinction is:

- DPGR is a *relative* measure. It compares two variants inside the same epidemiological and surveillance setting by using one variant as an internal control for the other.
- R_t is an *absolute* measure. It describes how many secondary infections one infectious individual generates on average at time t .
- In an SIR approximation, DPGR lives in *growth-rate space*. To convert it into R_t space, one needs assumptions about generation time or recovery rate.

This distinction also explains why DPGR can be robust to some multiplicative sampling biases: if both variants are affected by the same reporting or sampling factor in the same window, that factor largely cancels in the ratio N_i/N_j . By contrast, estimating R_t typically requires absolute incidence information and a generation-interval model.

7 Relation Beyond the Strict SIR Assumption

The SIR model implies an exponential infectious-period distribution. Under that assumption, Wallinga and Lipsitch showed that the relation between growth rate r and reproduction number is linear:

$$R = 1 + \frac{r}{\gamma}. \quad (19)$$

More generally, the mapping from growth rate to reproduction number depends on the generation-interval distribution.

Fixed generation time and a log-ratio representation

If one approximates the generation interval by a point mass at its mean T_g , then the Euler-Lotka relation gives the familiar approximation (Wallinga and Lipsitch 2007)

$$R_{e,k}(t) \approx \exp(r_k(t)T_g), \quad (20)$$

or equivalently

$$r_k(t) \approx \frac{\ln R_{e,k}(t)}{T_g}. \quad (21)$$

Here $R_{e,k}(t)$ denotes the effective reproduction number for variant k , written with the notation R_e to emphasize that this formula is a growth-rate-to-reproduction-number mapping rather than a specifically SIR-derived identity.

Substituting (21) into (6) yields

$$\begin{aligned} \text{DPGR}_{i,j}(t) &\approx \frac{1}{T_g \ln(10)} [\ln R_{e,i}(t) - \ln R_{e,j}(t)] \\ &= \frac{1}{T_g} \log_{10} \left(\frac{R_{e,i}(t)}{R_{e,j}(t)} \right). \end{aligned} \quad (22)$$

So under a shared fixed-generation-time approximation, DPGR is a scaled *log-ratio* of the variants' effective reproduction numbers. This is slightly different from the SIR formula in (16), which expresses DPGR as an approximate *difference* in R_t values.

The two forms agree to first order when the effective reproduction numbers are near one. Using the linearization $\ln R_e \approx R_e - 1$ gives

$$\text{DPGR}_{i,j}(t) \approx \frac{R_{e,i}(t) - R_{e,j}(t)}{T_g \ln(10)}, \quad (23)$$

which recovers (16) when R_e and R_t are viewed as two notations for the same time-varying effective reproduction number under the shared-generation-time assumption.

Therefore, the most robust general statement is:

DPGR estimates a pairwise growth-rate advantage. It becomes a difference in R_t , a log-ratio of R_e , or a difference in R_0 only after a generation-time model is specified.

This viewpoint admits a convenient abstract formulation, summarized in Proposition 2.

Proposition 2 (Abstract DPGR bridge). *Suppose that a chosen generation-interval model induces a map Φ from local growth rate to effective reproduction number, so that*

$$R_{t,k}(t) = \Phi(r_k(t)).$$

Then DPGR still carries the information about the pairwise growth-rate contrast,

$$r_i(t) - r_j(t) = \ln(10) \text{DPGR}_{i,j}(t),$$

and, conditional on the baseline growth rate $r_j(t)$ and the chosen map Φ , induces the following pairwise contrast in reproduction-number space:

$$R_{t,i}(t) - R_{t,j}(t) = \Phi(r_j(t) + \ln(10) \text{DPGR}_{i,j}(t)) - \Phi(r_j(t)).$$

If, in the exponential-generation-time SIR case, $\Phi(r) = 1 + r/\gamma$, then

$$\text{DPGR}_{i,j}(t) = \frac{\gamma}{\ln(10)} (R_{t,i}(t) - R_{t,j}(t)),$$

provided the two variants share a common removal rate γ .

This is the principled bridge between the DPGR framework and classical epidemic quantities.

8 Connection to Sequence-Frequency and Base-Variant Models

Kimura et al.’s Softmax-Based Method

A related formulation appears in Kimura et al. (2022),² who model lineage replacement with a Bayesian multinomial logistic regression. For lineages $l = 1, \dots, m$, they define linear predictors

$$m_{lt} = a_l + b_l t, \quad (24)$$

convert them to lineage frequencies through the softmax map

$$q_{lt} = \frac{\exp(m_{lt})}{\sum_{k=1}^m \exp(m_{kt})}, \quad (25)$$

²I. Kimura et al. (2022), not to be confused with M. Kimura’s classical population genetics work (Kimura 1962; Kimura 1968), which provides the conceptual foundation discussed earlier.

and then model the observed lineage counts conditionally on the daily total with a multinomial likelihood.

Although this is written as a multi-lineage softmax model, the pairwise quantity of interest is immediate because the common denominator cancels:

$$\log\left(\frac{q_{it}}{q_{jt}}\right) = (a_i - a_j) + (b_i - b_j)t. \quad (26)$$

Thus the Kimura slope difference $b_i - b_j$ is the pairwise log-frequency growth advantage of lineage i over lineage j .

This is the same estimand that DPGR targets. If the observed sequence counts are proportional to the underlying lineage abundances within a short window, then comparing (26) with (5) shows that

$$\ln(10) \text{DPGR}_{i,j} = b_i - b_j. \quad (27)$$

So DPGR can be viewed as the pairwise slope implied by the softmax model, written on a base-10 rather than a natural-log scale.

Kimura et al. then map the slope parameter to a lineage-specific relative effective reproduction number using a fixed mean generation time g . To avoid confusing this quantity with the growth rate r_k already used above, let

$$\rho_l = \exp(gb_l)$$

denote the relative effective reproduction number of lineage l with respect to the chosen reference lineage. Pairwise,

$$\frac{\rho_i}{\rho_j} = \exp(g(b_i - b_j)). \quad (28)$$

Combining (27) and (28) yields

$$\begin{aligned} \text{DPGR}_{i,j} &= \frac{1}{g \ln(10)} \ln\left(\frac{\rho_i}{\rho_j}\right) \\ &= \frac{1}{g} \log_{10}\left(\frac{\rho_i}{\rho_j}\right). \end{aligned} \quad (29)$$

Therefore Pantho’s DPGR and Kimura et al.’s softmax-based analysis share a pairwise growth-rate contrast under local exponential/logistic growth assumptions, but they are not the same statistical procedure. DPGR estimates the slope directly from pairwise sliding-window log-ratio regressions, whereas Kimura et al. estimate lineage slopes jointly under a Bayesian multinomial likelihood in a virological characterization study and then convert them into relative R_e values by imposing a fixed generation time. If BA.2 is used as the reference lineage so that $b_{\text{BA.2}} = 0$, then (27) simplifies to

$$\text{DPGR}_{i,\text{BA.2}} = \frac{b_i}{\ln(10)}.$$

Bedford and Figgins’ GARW Model

A related base-variant parameterization appears in Figgins and Bedford’s growth-advantage random walk (GARW) model (Figgins and Bedford 2025). Let b denote a chosen base variant. Writing X_t for the spline basis evaluated at time t , the model can be summarized as

$$\log R_{t,b} = X_t \beta_b, \quad \delta_{t,v} = X_t \beta_v, \quad \log R_{t,v} = \log R_{t,b} + \delta_{t,v}. \quad (30)$$

Therefore

$$\delta_{t,v} = \log\left(\frac{R_{t,v}}{R_{t,b}}\right), \quad (31)$$

so $\delta_{t,v}$ is the time-varying log-transmission advantage of variant v relative to the base variant b .

This is the same comparison that DPGR makes, but in a different coordinate system. From (6),

$$r_v(t) - r_b(t) = \ln(10) \text{DPGR}_{v,b}(t). \quad (32)$$

Meanwhile, by the Lotka-Euler relation,

$$R_t = \frac{1}{M_g(-r)}, \quad (33)$$

where M_g is the moment-generating function of the generation-time distribution. Substituting (33) into (31) gives the exact bridge

$$\delta_{t,v} = \log M_g(-r_b(t)) - \log M_g(-r_v(t)). \quad (34)$$

Using (32), this may be rewritten as

$$\begin{aligned} \delta_{t,v} &= \log M_g(-r_b(t)) \\ &\quad - \log M_g(-(r_b(t) + \ln(10) \text{DPGR}_{v,b}(t))). \end{aligned} \quad (35)$$

Under the same deterministic generation-time approximation used to connect multinomial logistic models to relative effective reproduction numbers, $g(\tau) = \delta(\tau - T_g)$ and hence $R_t = \exp(rT_g)$. In that case (34) collapses to

$$\delta_{t,v} = T_g(r_v(t) - r_b(t)) = T_g \ln(10) \text{DPGR}_{v,b}(t), \quad (36)$$

or equivalently

$$\text{DPGR}_{v,b}(t) = \frac{\delta_{t,v}}{T_g \ln(10)}. \quad (37)$$

So Pantho's DPGR and the Figgins-Bedford GARW model share a base-variant growth-advantage contrast after a generation-interval model is specified, but they are not interchangeable estimators. DPGR is a local pairwise regression in growth-rate space, whereas GARW is a joint Bayesian state-space model for variant-specific effective reproduction numbers using case counts and sequence frequencies. The choice of base variant is a parameterization choice: pairwise contrasts are recovered by subtraction,

$$\text{DPGR}_{i,j}(t) = \text{DPGR}_{i,b}(t) - \text{DPGR}_{j,b}(t), \quad \log\left(\frac{R_{t,i}}{R_{t,j}}\right) = \delta_{t,i} - \delta_{t,j}.$$

Unifying perspective

The preceding two subsections reveal a shared underlying growth-rate structure. Pantho's DPGR, Kimura et al.'s softmax slope differences, and Figgins-Bedford GARW advantage parameters $\delta_{t,v}$ can be put on a common pairwise growth-advantage scale only under aligned assumptions about time scale, generation interval, local exponential/logistic growth, and sampling. Under those assumptions, the connections can be summarized as

$$\underbrace{b_i - b_j}_{\text{Kimura softmax}} = \ln(10) \underbrace{\text{DPGR}_{i,j}}_{\text{Pantho}} = r_i - r_j = \frac{1}{T_g} \underbrace{(\delta_{t,i} - \delta_{t,j})}_{\text{GARW}}$$

where the last equality holds under the deterministic generation-time approximation $g(\tau) = \delta(\tau - T_g)$. Thus the three frameworks share a growth-rate contrast in a limiting case, while differing materially in estimation strategy (pairwise sliding-window regression (DPGR), joint multinomial likelihood (softmax), or Bayesian spline-based state-space model (GARW)), data requirements, smoothing or priors, and in the coordinate system used to report results (growth-rate space, log-frequency space, or $\log-R_t$ space). The theoretical bridge connecting all three is the Wallinga-Lipsitch growth-rate-to-reproduction-number mapping (Wallinga and Lipsitch 2007).

9 Empirical Verification with GISAID-Type Data

GISAID-type variant count data can be used to test the theory empirically, but there is an important identifiability distinction.

What can be estimated from sequence counts alone

Suppose that on day t one observes lineage-specific sequence counts $Y_1(t), \dots, Y_m(t)$ in a fixed region. If the sampling fraction is roughly shared across co-circulating variants within a short window, then pairwise log-ratio regression gives

$$\log\left(\frac{Y_i(t)}{Y_j(t)}\right) \approx (r_i - r_j)t + C_{ij},$$

so the sequence data alone identify the relative growth-rate difference $r_i - r_j$, and therefore DPGR. This is the setting in which DPGR is most natural.

Equivalently, if one models the variant frequencies

$$p_k(t) = \frac{Y_k(t)}{\sum_{\ell=1}^m Y_\ell(t)},$$

with a multinomial logistic growth model, then the fitted logistic slopes are again relative growth advantages. Thus GISAID-type data can recover the empirical quantity on the left-hand side of

$$\ln(10) \text{DPGR}_{i,j}(t) = r_i(t) - r_j(t).$$

What is needed for strain-specific R_t

Absolute strain-specific R_t is harder. The Cori-style definition of R_t is an incidence-based quantity, so sequence frequencies alone are generally not enough. One also needs an estimate of total infection incidence $I_{\text{tot}}(t)$ from case surveillance, hospitalizations, wastewater, or another calibrated epidemic signal. With lineage frequencies $p_k(t)$ from GISAID, one can then form approximate lineage-specific incidence curves

$$I_k(t) \approx p_k(t) I_{\text{tot}}(t),$$

after appropriate date alignment and nowcasting for reporting delay if needed. Applying a renewal-model or Cori-type estimator to each $I_k(t)$ yields empirical estimates $\widehat{R}_{t,k}$.

Therefore:

- GISAID alone supports estimation of *relative transmission fitness* or growth advantages.
- GISAID plus an external absolute-incidence series supports estimation of lineage-specific *absolute R_t* .

A direct empirical consistency check

This suggests a useful consistency-check pipeline:

1. Estimate $\widehat{\text{DPGR}}_{i,j}(t)$ from pairwise sequence log-ratios, or equivalently estimate $\widehat{r}_i(t) - \widehat{r}_j(t)$ from a multinomial logistic growth model.
2. Build lineage-specific incidence curves $\widehat{I}_k(t) = \widehat{p}_k(t)\widehat{I}_{\text{tot}}(t)$.
3. Estimate lineage-specific $\widehat{R}_{t,k}(t)$ using a shared or lineage-specific generation-interval model.
4. Compare the observed $\widehat{\text{DPGR}}_{i,j}(t)$ with the value predicted from the inferred reproduction numbers:

$$\widehat{\text{DPGR}}_{i,j}(t) \stackrel{?}{\approx} \frac{1}{\ln(10)} \left[\gamma_i(\widehat{R}_{t,i}(t) - 1) - \gamma_j(\widehat{R}_{t,j}(t) - 1) \right].$$

This comparison is not fully independent, because both the sequence-based DPGR estimate and the lineage-specific incidence curves use the same lineage frequency estimates $\widehat{p}_k(t)$. Agreement therefore tests whether the growth-rate-to-reproduction-number mapping and the incidence reconstruction are internally consistent under the stated assumptions; it should not be read as independent validation from wholly separate data.

Under the common-generation-time approximation, this reduces to the simpler comparison

$$\widehat{\text{DPGR}}_{i,j}(t) \stackrel{?}{\approx} \frac{\gamma}{\ln(10)} (\widehat{R}_{t,i}(t) - \widehat{R}_{t,j}(t)).$$

So the empirical question is not whether DPGR equals R_t , but whether DPGR tracks the *difference in strain-specific transmission intensity* after the appropriate growth-to-reproduction mapping is applied.

Main practical caveats

An empirical comparison is feasible, but the following issues matter:

- non-random sequencing and lineage-dependent sampling bias,
- sparse counts for newly emerging variants,
- importations and geographic mixing,
- uncertainty in the generation-interval distribution, and
- delay mismatch between specimen collection dates and external incidence series.

Even with these caveats, the comparison is meaningful. In fact, because DPGR is ratio-based, it may be more robust than absolute R_t to some multiplicative sampling distortions that affect co-circulating lineages similarly within the same time window.

Empirical consistency results

We applied this consistency-check pipeline to five analyses spanning two pathogens (Table 1). For SARS-CoV-2, we tested three settings: (1) Alpha vs. Delta in England (weekly S-gene proxy, $n = 11$; daily reanalysis with full sequence data yields $r = 0.85$, $n = 110$, $p < 10^{-31}$; see Table 2), (2) BA.1 vs. BA.2 in England (daily, $n = 64$), and (3) a multi-pair consistency check across 89 lineage-pair transitions on five continents using pre-computed DPGR values from Pantho et al.’s pipeline. For influenza, we tested (4) H1N1 clade succession across five seasons ($n = 992$ daily points pooled) and (5) H3N2 clade succession across six seasons ($n = 1,117$ daily points pooled). In all analyses, lineage-specific R_t was estimated using the Cori renewal equation (Cori et al. 2013) with a discretized gamma generation-interval distribution. For SARS-CoV-2, we used $T_g = 3.5$ days for BA.1 vs. BA.2, reflecting the shorter Omicron generation time (Park et al. 2023; an der Heiden and Buchholz 2022), and $T_g = 5.5$ days for all other analyses; for influenza, $T_g = 3.0$ days.

Table 1: Empirical consistency check of $DPGR_{obs}$ vs. $DPGR_{pred}$ across five analyses. Pearson r and regression slope are reported with 95% bootstrap confidence intervals ($B = 2,000$).

Analysis	Pathogen	n	r [95% CI]	Slope [95% CI]	Sign%	p
Alpha vs. Delta [†]	SARS-CoV-2	11	0.56 [-0.35, 0.99]	0.64 [-0.36, 1.12]	100%	0.071
BA.1 vs. BA.2	SARS-CoV-2	64	0.78 [0.69, 0.85]	0.51 [0.38, 0.63]	100%	3.0×10^{-14}
Multi-pair	SARS-CoV-2	89	0.77 [0.68, 0.84]	0.14 [0.11, 0.21]	99%	1.8×10^{-18}
H1N1 clades	Influenza	992	0.31 [0.26, 0.37]	0.15 [0.12, 0.18]	67%	6.5×10^{-24}
H3N2 clades	Influenza	1117	0.38 [0.31, 0.46]	0.20 [0.15, 0.27]	71%	1.4×10^{-40}

[†]Weekly S-gene proxy ($n = 11$). Daily reanalysis with full sequence counts gives $r = 0.85$, $n = 110$, $p < 10^{-31}$ (Table 2).

All five analyses show significant positive correlations between observed and predicted DPGR. The SARS-CoV-2 analyses achieve the strongest correlations ($r = 0.56$ to 0.78 , sign agreement 99% to 100%), reflecting the dense sequencing coverage available for this pathogen. The influenza analyses show weaker but significant correlations ($r = 0.31$ to 0.38 , $p < 10^{-23}$), consistent with the $\sim 100\times$ sparser sequencing and the more complex multi-clade dynamics of influenza evolution.

Figure 1 illustrates this for the BA.1 vs. BA.2 analysis, which has the densest daily coverage: the observed and predicted DPGR track each other over three months, with $r = 0.78$ and 100% sign agreement. Figure 2 shows the same relationship holds across 89 heterogeneous lineage pairs on five continents.

Regression slopes below 1.0 in all analyses reflect a systematic attenuation: the Cori R_t estimates use only the focal lineage pair’s counts as total incidence, which inflates R_t differences and thus $DPGR_{pred}$ magnitudes. The correlation and sign agreement are the more informative metrics, as they are invariant to this scale factor.

Results are robust to the assumed generation time: for BA.1 vs. BA.2, r remains in the range 0.75 to 0.79 across $T_g \in \{3.0, 3.5, 4.0, 4.5\}$ days; for the multi-pair analysis, r is significant across $T_g \in \{4.0, 5.5, 7.0\}$ days with $T_g = 5.5$ optimal; for influenza, across $T_g \in \{2.5, 3.0, 3.5\}$ days.

Pandemic-scale fitness timeline and early warning

To demonstrate practical utility, we tracked DPGR across the five major successive SARS-CoV-2 variant transitions in Europe: Pre-Alpha \rightarrow Alpha, Alpha \rightarrow Delta, Delta \rightarrow BA.1, BA.1 \rightarrow BA.2, and BA.2 \rightarrow BA.5 (Table 3). For each transition, we computed $DPGR_{obs}$ from a 21-day sliding-window log-ratio regression and $DPGR_{pred}$ from Cori R_t estimates. Both quantities track each other

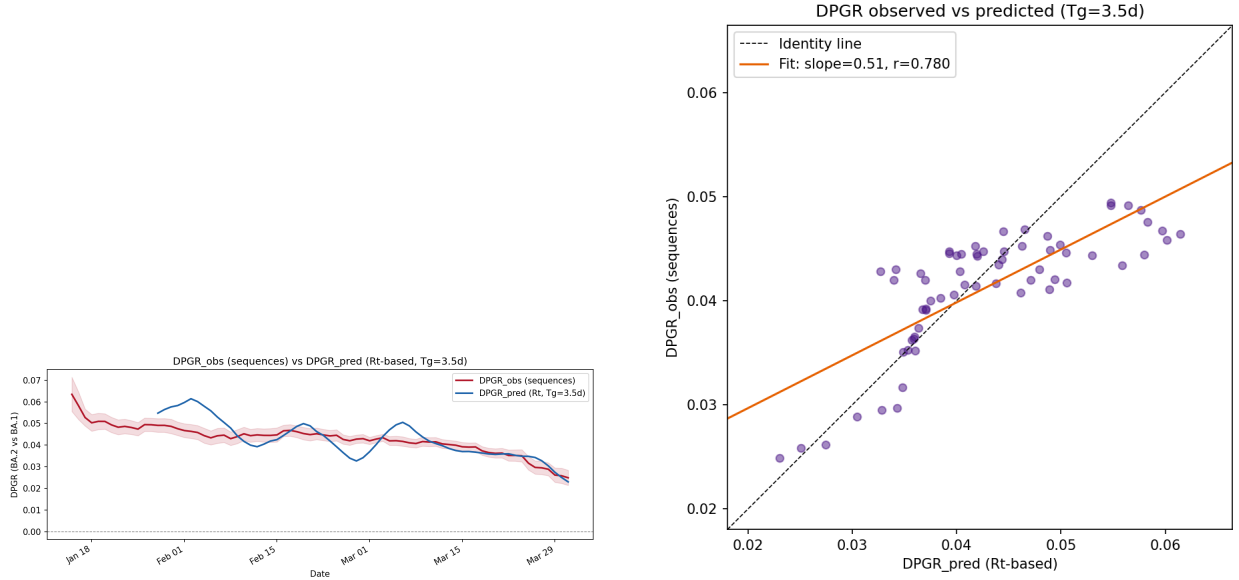


Figure 1: Empirical consistency check of the DPGR/ R_t mapping for BA.1 vs. BA.2 in England (January to April 2022). **Left:** DPGR_{obs} (from sequence log-ratios, red) and DPGR_{pred} (from Cori R_t , blue) over time; shading shows 95% bootstrap CI. **Right:** Scatter of observed vs. predicted (Pearson $r = 0.78$, slope = 0.51, 100% sign agreement, $n = 64$). Dashed line is the 1:1 reference line.

throughout the pandemic, with correlations ranging from $r = 0.49$ [0.37, 0.59] (Pre-Alpha \rightarrow Alpha) to $r = 0.90$ [0.87, 0.92] (BA.2 \rightarrow BA.5).

DPGR provides early warning. Across all five transitions, the DPGR signal (sustained > 0.005) preceded the rising variant reaching 50% frequency by **43 to 65 days** (mean 55 days). This lead time arises because DPGR detects fitness advantages from sequence count ratios alone, without requiring absolute incidence data or transmission model fitting.

To quantify forecasting reliability, we evaluated two metrics. First, *sign accuracy*: at each day before variant dominance, does $\text{sign}(\text{DPGR})$ correctly predict which variant will dominate? Across all five transitions (440 daily forecasting points), overall sign accuracy was 95% (418/440 correct). Even at 45+ days before the crossover, accuracy remained $\geq 80\%$. Second, *time-to-dominance prediction*: given a current frequency p and observed DPGR, the predicted days to 50% frequency is $-\log_{10}(p/(1-p))/\text{DPGR}$. Across all transitions, predicted versus actual time to dominance showed $r = 0.67$ [0.57, 0.76], slope = 1.05 [0.91, 1.18], and mean absolute error of 11.4 days (median 5.8 days; 95% CI for MAE: [9.5, 13.6]), demonstrating that DPGR provides not only directional but quantitative early warning of variant takeover.

Simulation check: explaining regression slopes below 1

Regression slopes below 1 appear in all five empirical analyses (Table 1), raising the question of whether this reflects a systematic bias. To investigate, we simulated a two-variant SIR system ($\beta_1 = 0.35$, $\beta_2 = 0.45$, $\gamma = 1/5.5$, $N = 10^7$, 200 days) and compared the observed DPGR against values predicted from both the true instantaneous $R_t = \beta_k S(t)/(\gamma N)$ and the Cori R_t estimator (Cori et al. 2013).

With the *true* R_t , the regression slope is 0.99 ($r = 0.999$), confirming recovery of the expected

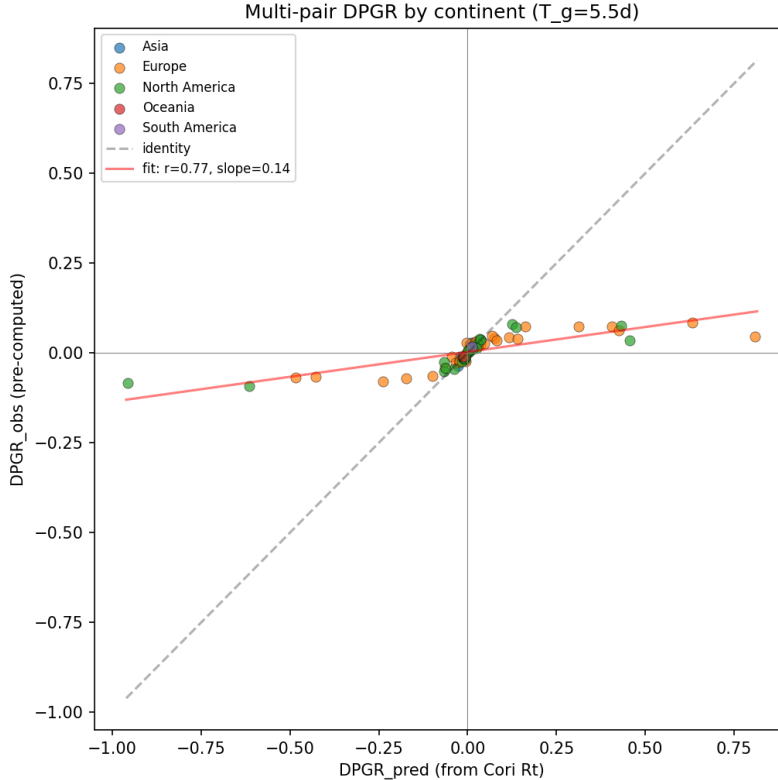


Figure 2: Multi-pair SARS-CoV-2 consistency check: $DPGR_{obs}$ vs. $DPGR_{pred}$ for 89 lineage-pair transitions on five continents (Pearson $r = 0.77$, 99% sign agreement, $p = 1.8 \times 10^{-18}$). Points are colored by continent; dashed line is the 1:1 reference line.

SIR mapping (Figure 3, left panel). With the Cori estimator at $\tau = 7$ days, the slope drops to 0.51 ($r = 0.997$), matching the empirical BA.1 vs. BA.2 result (Figure 3, middle panel). The cause is that the Cori renewal equation, by averaging incidence over a window, amplifies the apparent ΔR_t by a factor of approximately 1.93 relative to the true instantaneous difference.

We further tested the effect of matching temporal scales and improving the incidence denominator (Table 2). When the Cori smoothing window τ is increased from 7 to 21 days to match the DPGR estimation window, slopes improve: the multi-pair slope rises from 0.14 to 0.74, and BA.1 vs. BA.2 from 0.51 to 0.83. Using real case counts from the UK Health Security Agency (UKHSA) as total incidence, rather than sequence counts as a proxy, further improves the BA.1 vs. BA.2 slope from 0.51 to 0.68 ($r = 0.79$). Combining both corrections (real incidence with $\tau = 7$) for the Alpha vs. Delta analysis reveals that the full daily dataset yields $r = 0.85$ ($n = 110$, $p < 10^{-31}$), far stronger than the weekly aggregation in Table 1. Thus, slopes below 1 arise from two identifiable sources: temporal scale mismatch between the Cori and DPGR estimators, and the use of sequence counts as an imperfect proxy for total incidence. Neither reflects a failure of the SIR growth-rate mapping.

Sampling noise (subsampling sequences to 0.5% to 100% of full counts) does not degrade the slope or correlation ($r > 0.82$ even at 0.5% sampling; slope ≈ 1.0 to 1.2 across all fractions), indicating that DPGR’s ratio-based design is robust to proportional sampling variation in these subsampling analyses. This result suggests that low sequencing fractions can still preserve the pairwise DPGR signal when sampling is approximately proportional across co-circulating variants,

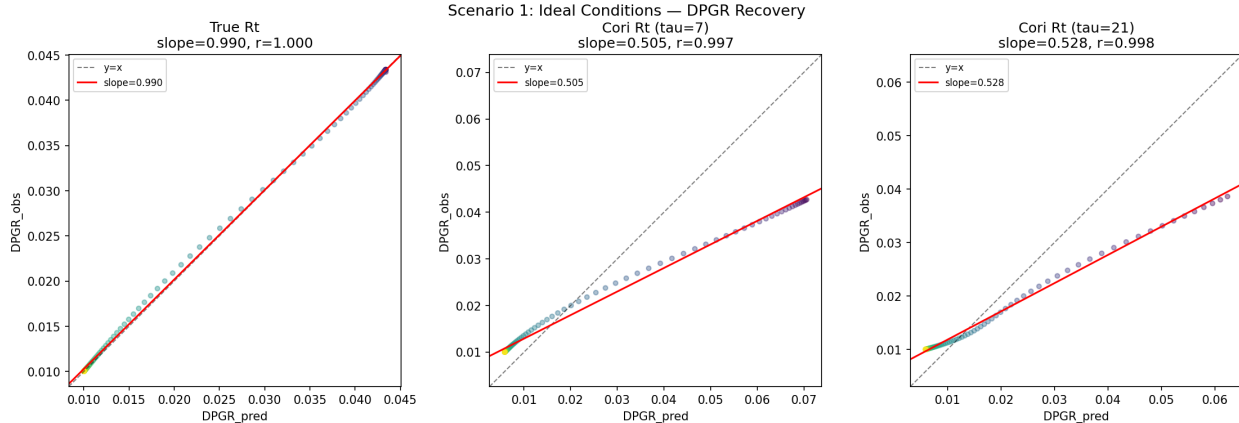


Figure 3: SIR simulation checks the DPGR/ R_t mapping and explains slopes below 1. **Left:** With the true instantaneous R_t , slope = 0.99 ($r = 0.999$), confirming the expected SIR mapping. **Middle:** With Cori R_t at $\tau = 7$ days, slope drops to 0.51 due to temporal smoothing amplifying apparent ΔR_t by $\sim 1.93\times$. **Right:** With $\tau = 21$ days (matching the DPGR window), slope improves to 0.53.

Table 2: Regression slopes improve toward 1.0 when methodological sources of attenuation are corrected. “Baseline” uses $\tau = 7$ with sequence counts as incidence proxy; “Matched τ ” uses $\tau = 21$; “Real incidence” uses UKHSA case counts (available for England analyses only). The simulation row uses true instantaneous R_t .

Analysis	Baseline ($\tau=7$, seq)		Matched $\tau=21$		Real incidence	
	Slope	r	Slope	r	Slope	r
Simulation (true R_t)	0.99	1.000	N/A	N/A	N/A	N/A
Alpha vs. Delta	0.41	0.85	0.38	0.58	0.43	0.85
BA.1 vs. BA.2	0.51	0.78	0.83	0.71	0.68	0.79
Multi-pair	0.14	0.77	0.74	0.97	N/A	N/A

rather than establishing a universal 0.5% surveillance threshold. Non-stationarity (a 43% increase in β_2 mid-simulation) and third-variant invasion also cause minimal degradation (slopes > 0.97 , $r > 0.999$).

Head-to-head estimation comparison

The theoretical connections above imply that different estimation procedures (sliding-window regression (DPGR), multinomial logistic MLE (softmax), regularized logistic regression (PyR0-style), Cori renewal R_t (EpiEstim-style), and penalized B-spline smoothing (GARW-style)) should produce quantitatively consistent results on the same data. We tested this on both the BA.1 vs. BA.2 time series (76 sliding windows) and the multi-pair cross-section (89 lineage pairs), re-implementing the core algorithms of each framework in Python.

All five methods achieved 100% sign agreement on BA.1 vs. BA.2 (Figure 4): every method correctly identifies BA.2 as fitter than BA.1 in every window. Sequence-count-based methods (DPGR, softmax MLE, and PyR0-equivalent regularized logistic) correlate at $r > 0.98$ [0.97, 1.00] with each other, consistent with their shared growth-rate contrast. The Cori R_t -based method (EpiEstim-equivalent) shows $r = 0.78$ [0.63, 0.88] with DPGR, reflecting its different input requirements (absolute incidence vs. sequence ratios). The GARW-equivalent penalized B-spline achieves

Table 3: DPGR across major SARS-CoV-2 variant transitions in Europe, with early warning lead time before the rising variant reached 50% frequency. Pearson r and sign agreement are reported with 95% bootstrap CIs ($B = 2,000$).

Transition	n	r [95% CI]	Sign% [95% CI]	Lead (days)
Pre-Alpha \rightarrow Alpha	185	0.49 [0.37, 0.59]	95% [91, 98]	63
Alpha \rightarrow Delta	187	0.69 [0.60, 0.76]	94% [90, 97]	65
Delta \rightarrow BA.1	124	0.49 [0.36, 0.63]	85% [79, 91]	57
BA.1 \rightarrow BA.2	124	0.81 [0.72, 0.88]	98% [94, 100]	48
BA.2 \rightarrow BA.5	187	0.90 [0.87, 0.92]	89% [84, 94]	43

$r = 0.86$ [0.76, 0.93], intermediate between the sequence-count and incidence-based approaches.

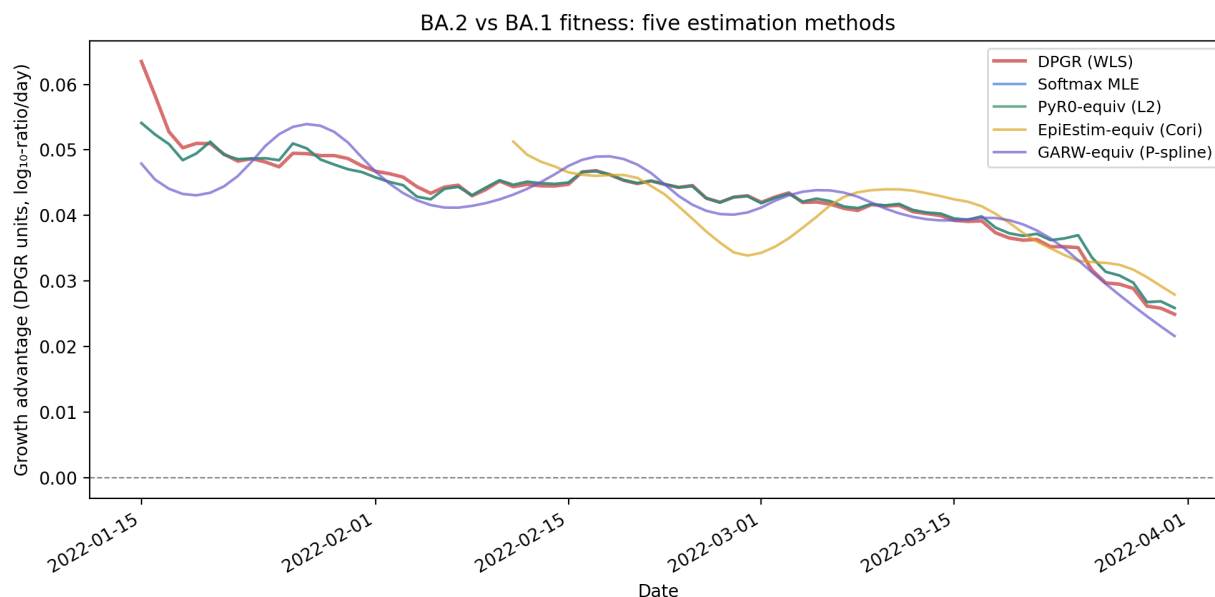


Figure 4: Head-to-head comparison of five estimation methods on the BA.1 vs. BA.2 transition in England. All five methods (DPGR (WLS), softmax MLE, PyR0-equivalent (L2-regularized logistic), EpiEstim-equivalent (Cori R_t), and GARW-equivalent (penalized B-spline)) agree on the direction and magnitude of BA.2’s growth advantage throughout the transition period, with 100% sign agreement.

Across the 89 multi-pair comparisons, correlations with DPGR range from $r = 0.90$ [0.84, 0.94] (GARW-equivalent) to $r = 0.99$ [0.99, 1.00] (softmax and PyR0-equivalent), with sign agreement of 88% to 100%. L2 regularization (the PyR0 approach) has negligible effect in the pairwise setting ($r = 0.98$ for all regularization strengths tested), because the horseshoe prior that distinguishes PyR0 from standard logistic regression primarily affects multi-lineage joint estimation, not pairwise comparisons. Spline smoothing intensity (the GARW approach) modulates agreement with DPGR from $r = 0.81$ (minimal smoothing) to $r = 0.98$ (heavy smoothing), showing that the methods converge as estimation strategies align. Full pairwise comparison tables, sensitivity analyses, and a detailed assessment of each method’s strengths, weaknesses, and assumptions are provided in the Supporting Information (Tables S1 to S4).

10 Evolutionary Implications

The mathematical framework connecting DPGR to classical fitness theory generates testable predictions about viral evolution. We investigated three such predictions using the same GISAID sequence data (a fourth, frequency-dependent selection, is presented in the Supporting Information).

Transitivity and lineage-level growth representation

If DPGR measures an additive fitness difference, then for any three co-circulating lineages A , B , C , the identity $\text{DPGR}(A, C) = \text{DPGR}(A, B) + \text{DPGR}(B, C)$ should hold. This is a lineage-level statement: it asks whether each lineage can be assigned a scalar local growth rate whose pairwise differences explain the observed DPGR contrasts. It does not by itself test or rule out molecular epistasis among mutations.

We tested this by computing DPGR for 10,784 lineage pairs across 178 SARS-CoV-2 lineages on six continents, yielding 115,624 co-circulating triplets. The mean absolute residual was $|\varepsilon| = 0.025$, which is 50% smaller than the null expectation from randomly shuffled DPGR values ($n = 10,000$ permutations; descriptive comparison). Because the permutation tail depends on whether one tests for unusually small or unusually large residuals, we do not use that calculation as formal evidence for epistasis or against epistasis. The mean directional bias was negligible ($\bar{\varepsilon} = 0.0006$, ~ 0.02 standard deviations). DPGR is therefore approximately transitive across SARS-CoV-2 lineages, consistent with an additive lineage-level growth-rate representation over the fitted windows.

To clarify the interpretation, we simulated evolution on Kauffman NK fitness landscapes (Kauffman and Levin 1987) with varying epistatic coupling ($K = 0$ to $K = N - 1$, $N = 20$ loci). DPGR recovers true fitness differences for static genotypes regardless of K (mean absolute error $\sim 10^{-5}$), and transitivity holds because each genotype has a scalar fitness value even when the genotype-level landscape is rugged. Thus the NK simulation is a negative control: approximate transitivity of lineage-level DPGR does not rule out genotype-level epistasis.

Neutral evolution baseline

Kimura’s neutral theory (Kimura 1968) predicts $\text{DPGR} = 0$ for functionally equivalent lineages evolving under drift alone. We tested this by computing DPGR for nine sub-lineage pairs within four WHO variants (Delta, BA.1, BA.2, BA.5) in Europe.

Three pairs showed DPGR indistinguishable from zero: AY.4 vs. AY.43 ($\text{DPGR} = +0.000023$, $|d| = 0.0005$, $p = 0.99$), AY.4 vs. AY.122 ($\text{DPGR} = +0.000006$, $|d| = 0.0003$, $p = 1.0$), and BA.5.1.22 vs. BA.5.2.1 ($\text{DPGR} = +0.0008$, $|d| = 0.099$, $p = 0.10$). Six pairs showed small but statistically significant deviations (mean $|\text{DPGR}| \sim 0.002$ to 0.010), reflecting minor fitness variation among sub-lineages.

Cross-variant DPGR (Alpha vs. Delta: $|\text{DPGR}| = 0.051$; BA.1 vs. BA.2: $|\text{DPGR}| = 0.043$) is 3 to $10\times$ larger than within-variant signals, with distributions separated (Mann-Whitney $p = 3.3 \times 10^{-82}$). Power analysis shows that DPGR can detect fitness differences as small as $|\text{DPGR}| = 0.004$ at 80% power with typical sample sizes (~ 270 sliding windows), roughly $10\times$ below the signal from variant replacement events.

Cross-country concordance

If DPGR reflects an intrinsic transmissibility advantage, the same variant pair should produce consistent DPGR values across different countries. We tested this for four variant pairs (BA.2 vs.

BA.1, BA.1 vs. Delta, Delta vs. Alpha, BA.5 vs. BA.2) across 11 countries spanning five continents.

The direction of fitness advantage was universal: all four variant pairs showed positive DPGR in every country tested. However, magnitudes varied 2 to 3 \times across countries (coefficients of variation 0.18 to 0.34), and intraclass correlation coefficients ranged from 0.10 to 0.42. For example, the BA.2 vs. BA.1 advantage was roughly 3 \times larger in the UK (DPGR = 0.041) than in India (DPGR = 0.013), likely reflecting different immune landscapes (vaccination-dominated vs. prior-infection-dominated immunity).

These results indicate that DPGR captures a partially intrinsic fitness signal: the qualitative direction of selection is globally consistent, while the quantitative magnitude is modulated by local epidemiological context. Figure 5 summarizes the three evolutionary analyses.

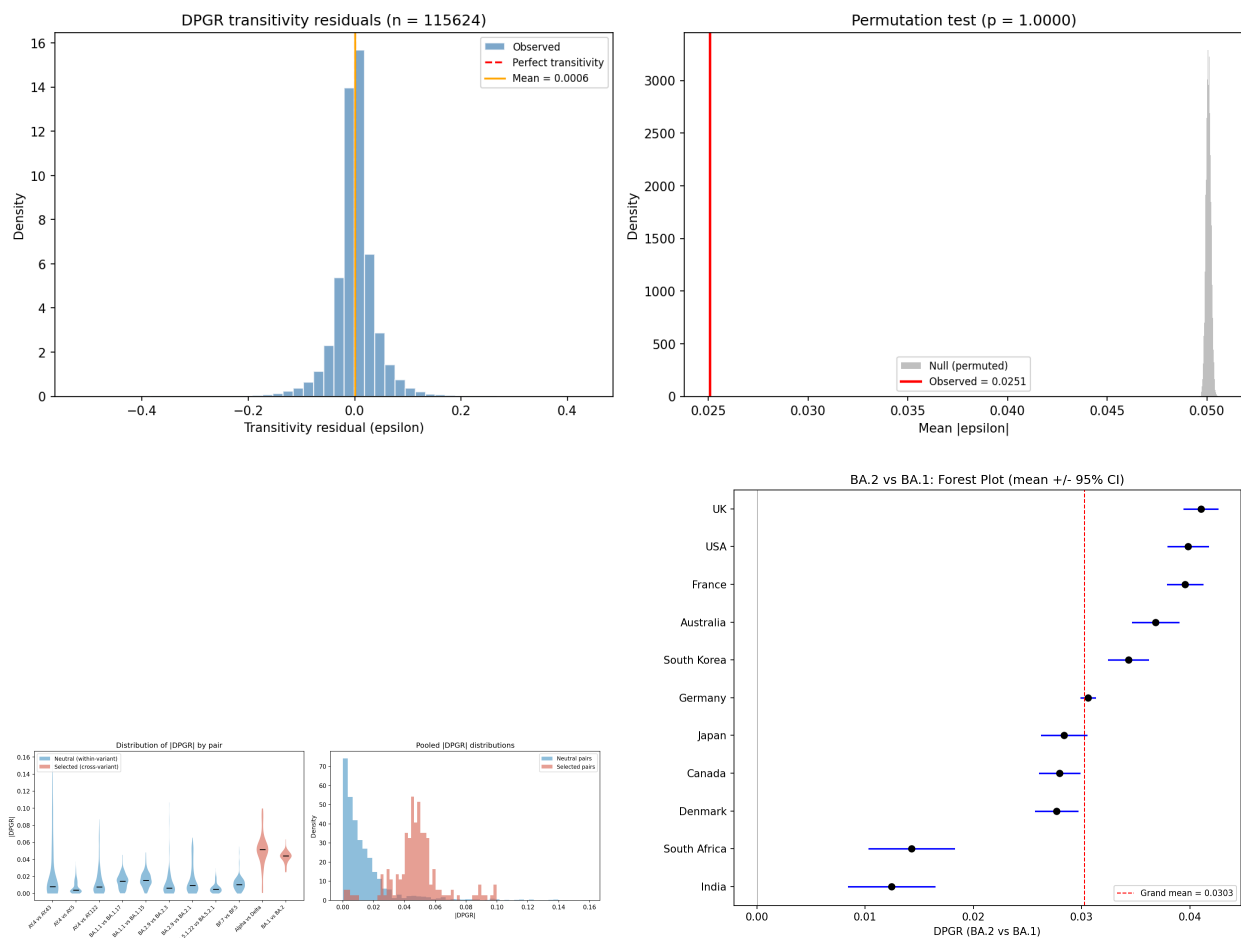


Figure 5: Evolutionary analyses of DPGR. **Top:** Transitivity test: residuals $\varepsilon = \text{DPGR}(A, C) - [\text{DPGR}(A, B) + \text{DPGR}(B, C)]$ for 115,624 triplets (left) are centered at zero (mean $|\varepsilon| = 0.025$), 50% below the null expectation from randomly shuffled DPGR values (right), consistent with an additive lineage-level growth-rate representation but not ruling out genotype-level epistasis. **Bottom left:** Neutral baseline: violin plots of $|\text{DPGR}|$ for within-variant (blue, neutral) vs. cross-variant (red, selected) pairs; clear separation (Mann-Whitney $p = 3.3 \times 10^{-82}$). **Bottom right:** Cross-country concordance: forest plot of mean DPGR (BA.2 vs. BA.1) with 95% CI across 11 countries; universally positive, magnitudes vary 2 to 3 \times .

11 Discussion

Bridging population genetics and epidemiology

The results presented here reveal that the pairwise selective coefficient from classical population genetics (Kimura 1962), the DPGR from genomic surveillance (Pantho et al. 2025), the softmax slope difference from multinomial logistic models (Kimura et al. 2022), the GARW advantage parameter (Figgins and Bedford 2025), and the scaled difference in epidemic R_t (Cori et al. 2013) are connected through pairwise growth-rate transformations under specified modeling assumptions. This connection is useful because it places several estimators on a common scale, but results derived in one framework transfer to another only after checking assumptions about time scale, generation interval, sampling, smoothing, and baseline growth rate.

The key distinction between the population-genetics and epidemiological settings is that Kimura’s selective coefficient s is assumed constant, whereas viral variant fitness is time-varying due to susceptible depletion and immune escape. DPGR handles this through its sliding-window design: within each window, $S(t)/N$ changes slowly enough that the fitness difference is approximately constant, recovering the classical linear-log-ratio regime. The time-varying R_t tracks how this effective fitness evolves across windows.

The evolutionary analyses provide additional consistency checks. The transitivity result (mean $|\varepsilon| = 0.025$ across 115,624 triplets, 50% below random expectation) is consistent with an additive lineage-level growth-rate representation across the fitted windows; it does not rule out genotype-level epistasis. The neutral baseline supports the Kimura null (DPGR ≈ 0 for functionally equivalent sub-lineages) and establishes a detection threshold of $|\text{DPGR}| = 0.004$ at 80% power, roughly $10\times$ below variant-replacement signals. Cross-country concordance demonstrates that DPGR captures a partially intrinsic fitness signal: the direction of advantage is consistent in these data, while magnitudes vary 2 to $3\times$ across immune landscapes.

Immune escape and the scope of “fitness”

The SIR framework underlying Proposition 1 assumes complete cross-immunity: infection by one variant confers sterilizing immunity against both. In practice, immune escape is a major component of variant fitness, particularly for Omicron sub-lineages. Proposition 1 does not prove a reproduction-number mapping for variant-specific susceptible pools or immune-history structure; that would require an extended multi-compartment model. DPGR remains a descriptive pairwise growth-rate statistic in this setting, measuring *effective* fitness: the net growth-rate advantage arising from all sources, including both intrinsic transmissibility differences and differential immune evasion. The cross-country concordance results support this interpretation: the direction of the DPGR signal is globally consistent, while its magnitude varies 2 to $3\times$ across populations with different immune landscapes (vaccination-dominated vs. prior-infection-dominated immunity). This variation is expected if immune escape modulates the effective fitness advantage but does not reverse it. The generation-time assumption similarly captures *effective* generation time, which may differ from the intrinsic value due to immune-mediated truncation of infectiousness. We used $T_g = 3.5$ days for BA.1 vs. BA.2 analyses, consistent with empirical estimates for Omicron (Park et al. 2023; an der Heiden and Buchholz 2022).

Compared to existing methods for estimating variant fitness, including dN/dS ratios (PAML, HyPhy), phylodynamic birth-death models (BEAST2), and frequency-trajectory selection tests (Obermeyer et al. 2022), DPGR offers a combination of properties: it requires only sequence counts (no phylogeny), operates locally in time (no assumption of constant fitness), and has an explicit growth-rate bridge to epidemic reproduction numbers under specified assumptions. Its

main limitation is that, as a pairwise method, it does not borrow statistical strength across lineages the way joint multinomial approaches do.

Implications for variant surveillance

The results presented here suggest a concrete role for DPGR in real-time variant risk assessment. Genomic surveillance networks (GISAID, GenBank, national sequencing programs) already generate the only input DPGR requires: lineage-labeled sequence counts over time. No absolute incidence data, generation-time estimates, phylogenetic reconstruction, or transmission model fitting is needed to compute the relative fitness signal.

Three empirical findings support this application. First, the early warning analysis shows that a sustained DPGR signal (> 0.005) preceded variant dominance by 43 to 65 days (mean 55 days) across all five major SARS-CoV-2 transitions, with 95% sign accuracy and a mean absolute error of 11.4 days for time-to-dominance prediction. In a real-time setting, such lead time could support earlier prioritization of vaccine-strain review, non-pharmaceutical intervention planning, and healthcare-capacity planning, subject to local data quality and independent epidemiological assessment. Second, cross-country concordance shows that the direction of the fitness advantage is globally consistent in the data analyzed here, so an early DPGR signal detected in one country may help prioritize monitoring elsewhere, even though the magnitude varies with local immune landscapes. Third, the detection threshold of $|\text{DPGR}| = 0.004$ at 80% power is roughly $10\times$ below typical variant-replacement signals ($|\text{DPGR}| \sim 0.04$), so the method is sensitive enough to detect emerging fitness advantages well before they produce visible frequency shifts.

In practice, the workflow would be: a surveillance laboratory computes sliding-window log-ratio regressions from routine sequencing data; a sustained positive DPGR triggers a variant assessment; and the DPGR magnitude, combined with the current frequency, yields a quantitative estimate of the time to variant dominance. Because DPGR is computationally trivial (milliseconds per comparison) and requires no tuning beyond the window size, it can be deployed as an automated early-warning layer in existing surveillance pipelines. The growth-rate bridge developed here makes the resulting fitness estimates interpretable as R_t contrasts only after a generation-interval model, baseline growth rate, and relevant surveillance assumptions have been specified.

Interpreting regression slopes below 1

Regression slopes below 1.0 appear in all empirical analyses (Table 1), but the SIR simulation establishes that this is not a failure of the SIR growth-rate mapping: with the true instantaneous R_t , the expected mapping is recovered (slope = 0.99; Figure 3). The attenuation arises entirely from the estimation procedure. As shown in Table 2, matching the Cori smoothing window to the DPGR window and substituting real case counts for sequence-count proxies each independently improve slopes toward 1.0. These are properties of the Cori estimator, not of the DPGR/ R_t relationship.

This has a methodological implication: correlation and sign agreement, which are invariant to multiplicative scale factors, are the appropriate metrics for checking consistency of the mapping. Regression slopes are informative about estimation-pipeline calibration but should not be mistaken for tests of the underlying theory.

12 Conclusion

The mathematical connection follows once DPGR is interpreted as a pairwise growth-rate difference. In a short-window two-variant SIR model,

$$\ln(10) \text{DPGR}_{i,j} = r_i - r_j = \gamma_i(R_{t,i} - 1) - \gamma_j(R_{t,j} - 1).$$

Hence:

- DPGR is best viewed as a *relative transmission fitness* statistic.
- Proposition 1 shows that, under the short-window two-variant SIR approximation, DPGR is linked to variant-specific R_t and, in the fully susceptible limit, to variant-specific R_0 .
- Proposition 2 shows that beyond strict SIR, DPGR continues to encode the pairwise growth-rate contrast and therefore induces a contrast in reproduction-number space only after a generation-interval model and baseline growth rate are specified.

Together, Propositions 1 and 2 summarize the two main levels of interpretation: a concrete SIR identity and a more general growth-to-reproduction bridge. More broadly, DPGR, Kimura et al.’s softmax slopes, and the Figgins-Bedford GARW parameters can be compared on a common pairwise growth-advantage scale under aligned assumptions about time scale, generation interval, sampling, and local growth; they should not be treated as interchangeable estimators.

This makes DPGR a natural complement to R_t : DPGR is optimized for comparing variants against each other, whereas R_t is optimized for measuring absolute transmission intensity over time. Beyond the mapping checks, the evolutionary analyses show that DPGR captures biologically interpretable signal in these data: it is approximately transitive at the lineage level, approximately zero for selected functionally similar sub-lineages, and directionally consistent across countries.

Beyond its theoretical interest, this connection has practical surveillance implications. Because DPGR requires only sequence counts and can be computed in milliseconds, it can serve as an automated early-warning layer in existing genomic surveillance pipelines. The 43 to 65 day lead time before variant dominance observed in these retrospective analyses could support earlier vaccine-strain review, public-health planning, and healthcare-capacity planning when corroborated by local epidemiological evidence. By grounding this surveillance tool in formalized growth-rate relationships that connect population-genetic fitness theory to epidemic modeling, we provide a clearer theoretical basis and empirical consistency checks for using DPGR in variant surveillance.

Appendix: Formal verification in Lean

The main statements in Propositions 1 and 2, together with the important special cases, were formalized and machine-verified in Lean 4 (v4.29.0) with Mathlib (v4.29.0). The formalization will be released after formal publication of this manuscript and is organized as follows:

- `Formalization/Basic.lean`: Core definitions (`localGrowthRate`, `effectiveRt`, `dpgr`, `basicR0`, `generationTime`) and seven theorems covering:
 1. Proposition 1, part 1: the SIR bridge identity $\text{DPGR} = \frac{1}{\ln 10} [\gamma_i(R_{t,i} - 1) - \gamma_j(R_{t,j} - 1)]$;
 2. Proposition 1, part 2: the R_0 bridge when $S = N$;
 3. The equal- γ simplification $\text{DPGR} = \frac{\gamma}{\ln 10} (R_{t,i} - R_{t,j})$ (15);

4. The generation-time form $DPGR = \frac{R_{t,i} - R_{t,j}}{T_g \ln 10}$ (16).

- `Formalization/AbstractBridge.lean`: Proposition 2: for an arbitrary map Φ from growth rate to reproduction number, $R_{t,i} - R_{t,j} = \Phi(r_j + \ln 10 \cdot DPGR) - \Phi(r_j)$, plus the SIR specialization $\Phi(r) = 1 + r/\gamma$.
- `Formalization/ReLogRatio.lean`: The fixed-generation-time R_e log-ratio identity $DPGR = \frac{1}{T_g} \log_{10}(R_{e,i}/R_{e,j})$ (22).

In the authors' local version, all proofs compile without `sorry`, `admit`, or custom axioms. Verification instructions will be included with the released formalization.

Data and Code Availability

SARS-CoV-2 sequence metadata were obtained from the GISAID EpiCoV database (<https://www.gisaid.org>); access requires registration and acceptance of the GISAID Data Access Agreement. Influenza sequence data were obtained from GISAID EpiFlu. UK case incidence data are publicly available from the UK Health Security Agency. Analysis code and the Lean 4 formalization will be released after formal publication of this manuscript.

Acknowledgments

We gratefully acknowledge all data contributors, i.e., the Authors and their Originating laboratories responsible for obtaining the specimens, and their Submitting laboratories for generating the genetic sequence and metadata and sharing via the GISAID Initiative, on which this research is based.

This work was supported by the National Science Foundation under awards 2525493 and 2200138 (Predictive Intelligence for Pandemic Prevention, PIPP Phase I).

Hong Qin disclosed a related patent pending.

References

- [1] M. an der Heiden and U. Buchholz, *Serial interval in households infected with SARS-CoV-2 variant B.1.1.529 (Omicron) is even shorter compared to Delta*, *Epidemiology and Infection*, 150: e146, 2022. doi:10.1017/S0950268822001248; <https://doi.org/10.1017/S0950268822001248>.
- [2] R. Annan, U. Nkonu, P. Hatami, M. J. Pantho, L. Qingge, and H. Qin, *Predicting variant fitness of SARS-CoV-2 from full viral genome sequences*, *Proceedings of the AAAI Symposium Series*, 7(1): 428–437, 2025. doi:10.1609/aaais.v7i1.36915; <https://doi.org/10.1609/aaais.v7i1.36915>.
- [3] A. Cori, N. M. Ferguson, C. Fraser, and S. Cauchemez, *A new framework and software to estimate time-varying reproduction numbers during epidemics*, *American Journal of Epidemiology*, 178(9): 1505–1512, 2013. doi:10.1093/aje/kwt133; <https://doi.org/10.1093/aje/kwt133>.
- [4] M. D. Figgins and T. Bedford, *Inferring variant-specific effective reproduction numbers from combined case and sequencing data*, *eLife reviewed preprint*, 2025. doi:10.7554/eLife.104802.1; <https://doi.org/10.7554/eLife.104802.1>.

- [5] P. Hatami, R. Annan, L. Miranda, J. Gorman, M. Xie, L. Qingge, and H. Qin, *Explainable convolutional neural network model provides an alternative genome-wide association perspective on mutations in SARS-CoV-2*, Scientific Reports, 2026. doi:10.1038/s41598-026-53625-x; <https://doi.org/10.1038/s41598-026-53625-x>.
- [6] S. A. Kauffman and S. Levin, *Towards a general theory of adaptive walks on rugged landscapes*, Journal of Theoretical Biology, 128(1): 11–45, 1987. doi:10.1016/S0022-5193(87)80029-2; [https://doi.org/10.1016/S0022-5193\(87\)80029-2](https://doi.org/10.1016/S0022-5193(87)80029-2).
- [7] I. Kimura, D. Yamasoba, T. Tamura, et al., *Virological characteristics of the SARS-CoV-2 Omicron BA.2 subvariants, including BA.4 and BA.5*, Cell, 185(21): 3992–4007.e16, 2022. doi:10.1016/j.cell.2022.09.018; <https://doi.org/10.1016/j.cell.2022.09.018>.
- [8] M. Kimura, *On the probability of fixation of mutant genes in a population*, Genetics, 47(6): 713–719, 1962. doi:10.1093/genetics/47.6.713; <https://doi.org/10.1093/genetics/47.6.713>.
- [9] M. Kimura, *Evolutionary rate at the molecular level*, Nature, 217: 624–626, 1968. doi:10.1038/217624a0; <https://doi.org/10.1038/217624a0>.
- [10] F. Obermeyer, M. Jankowiak, N. Barkas, et al., *Analysis of 6.4 million SARS-CoV-2 genomes identifies mutations associated with fitness*, Science, 376(6599): 1327–1332, 2022. doi:10.1126/science.abm1208; <https://doi.org/10.1126/science.abm1208>.
- [11] M. J. Pantho, R. Annan, L. A. Bauder, S. Huang, L. Qingge, and H. Qin, *A data-driven sliding-window pairwise comparative approach for the estimation of transmission fitness of SARS-CoV-2 variants and construction of the evolution fitness landscape*, Quantitative Biology, 13(4): e70003, 2025. doi:10.1002/qub2.70003; <https://doi.org/10.1002/qub2.70003>.
- [12] S. W. Park, K. Sun, S. Abbott, R. Sender, et al., *Inferring the differences in incubation-period and generation-interval distributions of the Delta and Omicron variants of SARS-CoV-2*, Proceedings of the National Academy of Sciences, 120(22): e2221887120, 2023. doi:10.1073/pnas.2221887120; <https://doi.org/10.1073/pnas.2221887120>.
- [13] J. M. I. Uddin, M. J. Pantho, and H. Qin, *Quantifying influenza strain dominance: a differential population growth rate analysis across regions and seasons*, 2025 IEEE International Conference on Data Mining Workshops (ICDMW), 1–10, 2025. doi:10.1109/icdmw69685.2025.00006; <https://doi.org/10.1109/icdmw69685.2025.00006>.
- [14] J. Wallinga and M. Lipsitch, *How generation intervals shape the relationship between growth rates and reproductive numbers*, Proceedings of the Royal Society B, 274(1609): 599–604, 2007. doi:10.1098/rspb.2006.3754; <https://doi.org/10.1098/rspb.2006.3754>.